

Fate of Quadratic Band Crossing under Quasi-Periodic Modulation

Raul Liquito¹, Miguel Gonçalves^{1,2}, Eduardo V. Castro^{1,3}

¹*Centro de Física da Universidade do Porto, Departamento de Física e Astronomia, Faculdade de Ciências, Universidade do Porto, 4169-007 Porto, Portugal*

²*CeFEMA, Instituto Superior Técnico, Universidade de Lisboa, Av. Rovisco Pais, 1049-001 Lisboa, Portugal and*

³*Beijing Computational Science and Research Center, Beijing 100084, China*

We study the fate of a two-dimensional quadratic band crossing topological phases under a one-dimensional quasi-periodic modulation. By employing numerically exact methods, we fully characterize the phase diagram of the model in terms of spectral, localization, and topological properties. Unlike in the presence of regular disorder, the quadratic band crossing is stable to the application of the quasi-periodic potential, as well as most of the topological phase transitions occur through a gap-closing and reopening mechanism, as in the homogeneous case. For sufficiently high quasi-periodic potential, the quadratic band crossing point splits into Dirac cones enabling transitions into gapped phases with Chern numbers $C = \pm 1$, absent in the homogeneous limit. This behavior stands in sharp contrast with the disordered case, where gapless $C = \pm 1$ phases can arise by perturbing the band crossing with any amount of disorder. In the quasi-periodic case, we find that the $C = \pm 1$ phases can only become gapless for higher potential strength. Only in this regime do the subsequent quasi-periodic-induced topological transitions into the trivial phase mirror the well-known “levitation and annihilation” mechanism in the disordered case.

I. INTRODUCTION

The unique characteristics of topological insulators compared to conventional band insulators have rendered them a central topic of current research [1–4]. The groundbreaking discovery of the quantum Hall effect [5] and its subsequent theoretical explanation through the lens of topology [6, 7] paved the way for the proposal of the quantum anomalous Hall effect Haldane [8]. Remarkably, these systems can exhibit a topological phase while no uniform magnetic field is applied and were realized experimentally in various platforms [9–12]. These so-called Chern insulators [4] arise from opening non-trivial gaps in systems with band crossing points carrying a finite quantized Berry phase, which can be accomplished by breaking time-reversal symmetry. The simplest and more extensively studied case of a band crossing point is that of a Dirac point, that hosts a low-energy linear dispersion described by a Dirac Hamiltonian, as it is the case for nodal superconductors and graphene [13]. Dirac points contain Berry phases of $\pm\pi$, but there are other possibilities for band crossings and associated Berry phases, as is the case of quadratic band crossing points (QBCPs). Two-dimensional systems with QBCPs are also of high interest because, on the one hand, they transport a finite Berry phase of $\pm 2\pi$ and on the other, a finite density of states at QBCP, contrary to Dirac points, renders these systems unstable to interactions [14]. In QBCP systems, interactions can induce nematic phases with two Dirac cones, each carrying half of the QBCP’s Berry phase, or gap openings that may give rise to topological insulating phases [15–18].

Even though topological band theory is studied in

momentum-space for translational invariant systems, topological insulators are known to be robust to the effects of uncorrelated disorder Xiao *et al.* [19]. In fact, disorder is a key ingredient for the observation of quantized Hall conductivity for quantum Hall systems since it localizes every state except those responsible for the quantized Hall current that live at very narrow energy windows [20–22]. In this way, varying the Fermi level in the gap filled with localized states cannot change the Hall conductivity, giving rise to a filling-independent plateau. Sufficiently large disorder, however, generically suppresses the topological properties by inducing a topological phase transition into a trivial phase, where the topological extended states meet and become suppressed through the “levitation and annihilation” mechanism [22–25]. However, numerous examples of disorder-induced topological phases, known as topological Anderson insulators, have also been found [26–31].

A different class of systems that break translational invariance, where more exotic localization properties can occur, are quasi-periodic systems. Contrary to disordered systems, extended, localized and critical multifractal phases can arise even in one-dimensional (1D) [32–40]. In higher dimensions, these systems have received considerable attention on the interplay between moiré physics and localization [41–49]. Systems with quasi-periodic modulations can be realized in widely different platforms, including optical lattices [50–59], photonic [48, 60–65] and phononic [66–71] metamaterials, and moiré materials [72–74]. The impact of quasi-periodic modulations on parent topological systems has also been previously studied [75–78], and was found to give rise to interesting topological phases with more complex localization prop-

erties than in the disordered cases.

The fate of a QBC in the presence of disorder was numerically studied in Ref. [79], in the non-interacting limit, where it was found to be unstable to the formation of topological insulating phases with Chern numbers $C = \pm 1$, not present in the model's clean limit. The interplay between disorder and interactions was also studied in Refs. [80, 81] by renormalization-group methods, where the interaction-induced topological insulating phases were found to be suppressed at strong disorder. The influence of quasi-periodic modulations on QBCP has, however, remained poorly explored so far, with the notable exception of Ref. [82]. In this reference, a quasi-periodic potential was applied to a QBCP system, that was found to be stable up to a flatband regime at which the wave function becomes delocalized in momentum-space, closely related to the incommensurate magic-angle regime found in moiré systems [46, 47, 83]. The study of the topological phases that can be induced by applying quasi-periodic modulations to a QBCP system has however remained unexplored up to now.

In this work, we study the topological and localization properties of a QBCP model with an applied 1D quasi-periodic modulation. The main results are in Fig. 1. The QBCP is robust for a small quasi-periodic potential, with the phase diagram remaining essentially unchanged concerning the homogeneous limit, as seen in Fig. 1(a). For higher quasi-periodic potential strength, phases with Chern numbers $C = \pm 1$, not present in the homogeneous limit, arise. The topological transitions into these phases occur through the gap closing and reopening mechanism, as shown in Fig. 1(b), being therefore of a different nature from the ones found in the disordered system in Ref. [79]. Interestingly, in most of the studied topological transitions, the gap closes at the same momentum as in the homogeneous case: at the center and corners of the first Brillouin zone (FBZ), defined in the translationally invariant direction. In Fig. 1(c), the localization length at the Fermi energy, obtained by the transfer matrix method, is seen to diverge at the gap-closing phase transitions. Away from the Fermi energy, we found large clusters of bulk extended states both in topological and trivial phases. This behavior contrasts with the disordered case, where all eigenstates are localized within the topological phases except for topologically non-trivial states that appear at specific energies. Only for an even higher potential do the $C = \pm 1$ phases can become gapless and exhibit similar physics to the disordered case. Further increasing the potential induces a transition into a trivial phase that mirrors typical topological transitions in the presence of disorder: close to the transition, topologically non-trivial extended states arise only at very narrow energy windows, merging at the transition, after which all states become trivial and localized, as in the “levitation and annihilation” mechanism [22–25].

The paper is organized as follows: In Sec. II, we intro-

duce the tight-binding model used to describe the electronic properties of the quasi-periodic QBC system and the methods to analyze its properties. In Sec. III we discuss the topological, spectral, and localization properties. In Sec. IV we give a thorough discussion of the

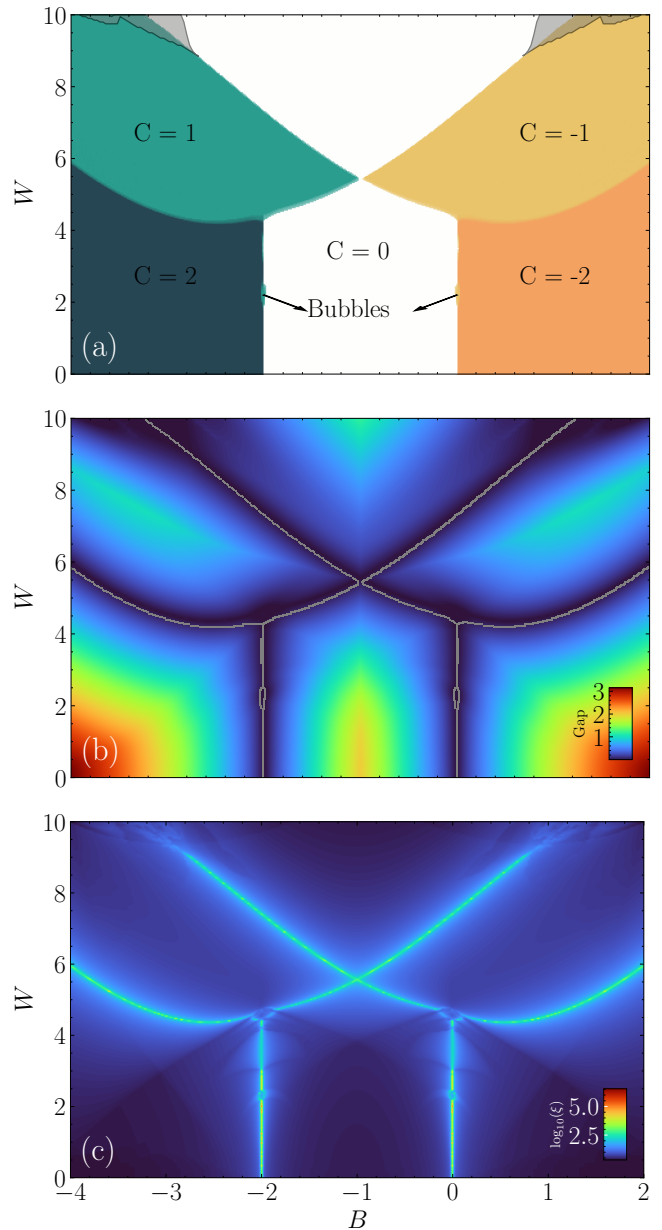


FIG. 1. (a) Chern number as a function of the model parameter B and quasi-periodic potential W for a system size of $L = 21$ and 20 different twists realizations. The greyed out areas are gapless. (b) Energy gap as a function of B and W for $L_y = 1597$. No twist realizations were considered. The grey lines represent the lines at which a topological phase transition occurs. (c) Localization length (ξ) at the Fermi level ($E = 0$) for the k_x values where the gap closes. A 1D system size of $N = 30000$ was used. The grid discretization is 300×300 .

obtained results. We also include three appendices: in Appendix A we provide the real space TB Hamiltonian and the k_x -dependent model; in Appendix B we present the Golden Ratio method used to compute the extrema of the energy spectrum; finally IPR and fractal dimension results are presented in Appendix C.

II. MODEL AND METHODS

We consider a QBCP model on a square lattice with two orbitals per unit cell [79]. This model is defined by the following clean limit \mathbf{k} -space Hamiltonian

$$\mathcal{H}_0 = \sum_{\mathbf{k}} \Psi_{\mathbf{k}}^\dagger \mathcal{H}_{\mathbf{k}} \Psi_{\mathbf{k}}, \quad (1)$$

where $\Psi_{\mathbf{k}}^\dagger = \begin{pmatrix} c_{\mathbf{k},A}^\dagger & c_{\mathbf{k},B}^\dagger \end{pmatrix}$, with $c_{\mathbf{k},\alpha}^\dagger$ the creation operator of a state with crystal momentum \mathbf{k} in the α orbital and

$$\mathcal{H}_{\mathbf{k}} = \mathbf{h}(\mathbf{k}) \cdot \boldsymbol{\sigma}, \quad (2)$$

with $\boldsymbol{\sigma}$ the vector of Pauli matrices and the vector $\mathbf{h}(\mathbf{k})$ given by

$$\begin{aligned} h_x &= 2t_x \sin(k_x) \sin(k_y) \\ h_y &= 0 \\ h_z &= 2t_z (\cos(k_x) - \cos(k_y)). \end{aligned} \quad (3)$$

From this point on, we set $t_x = t_y = t = 1$, so that every physical observable with energy units come in units of t .

QBCPs with symmetric Berry curvatures occur at $\Gamma = (0, 0)$ and $M = (\pm\pi, \pm\pi)$ points of the FBZ. For $h_y = 0$, the system is gapless, having a finite DOS at the Fermi level ($E = 0$). The introduction of a non-zero h_y perturbation opens a gap that can give rise to Chern insulating phases. This can be accomplished by introducing the following h_y term,

$$h_y = 1 + \frac{B+1}{2} (\cos(k_x) + \cos(k_y)). \quad (4)$$

For this model, a single QBCP occurs at M for $B = 0$, and for $B = -2$ at Γ . These are the only values of B for which the system becomes gapless, where topological phase transitions between phases with $C = 2 \leftrightarrow C = 0$ ($B = -2$) and $C = 0 \leftrightarrow C = -2$ ($B = 0$) take place (see Fig. 1(a), for $W = 0$).

In this work, we will study the fate of the model's phase diagram upon the addition of a 1D quasi-periodic potential. We consider the Aubry-André unidirectional potential given by the real-space Hamiltonian,

$$\mathcal{H}_W = \frac{W}{2} \sum_{\mathbf{R}, \alpha} \cos(2\pi\beta n) c_{\mathbf{R}, \alpha}^\dagger c_{\mathbf{R}, \alpha}, \quad (5)$$

where $\mathbf{R} = ma\hat{e}_x + na\hat{e}_y$ is a lattice vector and β is the potential frequency. In the thermodynamic limit we choose β to be an irrational number in order to break translational invariance; we choose the golden ratio $\beta = \phi_{\text{GR}} = (1 + \sqrt{5})/2$. We carried out numerical simulations for finite systems with $L_x = L_y = L$ (with L the number of unit cells in each direction) and periodic/twisted boundary conditions. In order to avoid boundary defects we have chosen system sizes $L \rightarrow L_n = F_n$, where F_n is the n -th order Fibonacci number, and approximated β with rational approximants of the golden ratio $\beta \rightarrow \beta_n = F_{n+1}/F_n$. This choice ensures that the system's unit cell is of size L , which guarantees that the system always remains incommensurate as L is increased. The potential in Eq. (5) keeps the system translational invariant along the x direction, and we take the Fourier transform along this direction to obtain \mathcal{H}_{k_x} , an Hamiltonian diagonal in Bloch momentum k_x (see Appendix A).

In what follows, we carry out an extensive study of the spectral, topological, and localization properties of the model. We compute the Chern number phase diagram of the system via the coupling matrix method of Ref. [84] as implemented in Ref. Zhang *et al.* [85]. Spectral properties were studied using exact diagonalization (ED) and the kernel polynomial method [86].

The transfer matrix method (TMM), introduced in [87, 88], can be used to compute the localization length and, therefore, to study bulk localization properties. At topological phase transitions, the states are extended at the Fermi level, while in topological phases, the system is either gapped or populated with localized states around the Fermi level. For the two last cases, the localization length at the Fermi level is finite, while in the former, it diverges in the thermodynamic limit. We also used TMM to cross-check the topological phase diagram obtained through Chern number calculations.

Throughout this work, we also realized averages over twisted boundary conditions, such that the phase twist followed a random uniform distribution in the interval $\theta_i \in [0, 2\pi[$. To apply phase twists the boundaries are periodically closed (as for periodic boundary conditions) but with an additional phase twist, so that:

$$\psi_\alpha(\mathbf{R} + L\mathbf{a}_i) = e^{i\theta_i} \psi_\alpha(\mathbf{R}), \quad (6)$$

where $\psi_\alpha(\mathbf{R}) = c_{\mathbf{R}, \alpha}^\dagger |0\rangle$. As the system approaches thermodynamic limit, any dependence on phase twists should vanish.

III. RESULTS

A. Topological Properties

We start by characterizing the topological phase diagram, shown in Fig. 1(a). The phase diagram was obtained for a system with 21×21 unit cells averaged over 20 random phase twists with twisted boundary conditions.

The clean limit presents topological transitions from $C = \pm 2$ to $C = 0$, with the gap closing at a QBCP ($B = \{-2, 0\}$). These transitions are robust for small W , still occurring at $B = \{-2, 0\}$. The observed behavior contrasts with the case of uncorrelated disorder, studied in Ref. [79], where it is shown that for infinitesimal disorder strength W , $C = \pm 1$ phases appear. For the present case of an incommensurate potential, $C = \pm 1$ phases only appear at large enough potential strength, indicating a different phenomenology. Interestingly, along the lines of fixed $B = -2, 0$, when the QBCP occurs, we see the appearance of small $C = \pm 1$ bubbles, indicated by the arrows in Fig. 1(a). These bubbles are also present in Fig. 1(b) for the gap and 1(c) for the localization length, which were obtained with very different system sizes, confirming they are not merely a result of finite-size effects.

Increasing the quasi-periodic potential along the lines of fixed $B = \{-2, 0\}$, it will be shown below that for $W \in [3.0, 4.5]$, the QBCP splits into two Dirac cones, and, eventually, at $W \approx 4.5$ a topological phase transition into $C = \pm 1$ phase occurs. For high enough potential strength, the remaining topological phases are suppressed, and the system transitions into a trivial phase. Unlike in the disordered case, there are both gapped and gapless $C = \pm 1$ phases separated by the thin black lines in Fig. 1(a), as we will detail below. As we will show, these quasi-periodic-induced phases are different from topological Anderson insulator phases that exist for uncorrelated disorder due to their distinct localization properties.

B. Gapped/Gapless Regions

To study the spectral gap of the system, we computed the closest eigenvalue to $E = 0$, which we call ϵ_{0+} , using the k_x -dependent model presented in Appendix A. We then estimate the gap of the system as $2\epsilon_{0+}$, which is well justified due to the particle-hole symmetry of the model, which ensures the spectrum is symmetric around $E = 0$.

In Fig. 1(b), we present the gap of the system, which was obtained using Lanczos decomposition alongside the shift invert method for $L_y = 1597$ at the value of k_x where the gap closes. Generally, we do not know the value of k_x at which the gap closes [89]. For this reason, a golden ratio search algorithm (see Appendix. B) was implemented

to compute the value of k_x that maximizes the valence band energy that corresponds to the gap closing point.

We can see in Fig. 1(b) that the gap closes and reopens in most topological phase transitions. We also see the appearance of gapless regions for strong potential, seen as wider blackish regions at high W . In Fig. 1(a) the greyed out regions were computed using the data in Fig. 1(b). Since the spectrum of a finite system is always discrete, we need to properly define a threshold gap value δ below which we consider the system to be gapless, chosen as the minimum value of the gap at well-defined gap closing and reopening topological transitions. For the considered system size, this value is $\delta \approx 0.015$.

C. Localization Properties

To complete the characterization of the phase diagram, we now turn to the study of the localization properties. We start by discussing the localization length (ξ) at the Fermi level ($E = 0$), obtained through the TMM, and shown in Fig. 1(c).

From the gap results presented in Fig. 1(b), we know that for most of the topological phase transitions the gap closes and reopens. Since the gap closing point should contain extended states at a topological phase transition, the localization length ξ should diverge at these points while remaining finite in the gapped regions. We can, therefore, capture the topological transitions by computing ξ as a function of B and W , as shown in Fig. 1(c).

Using the k_x -dependent model, we can reach closer to the thermodynamic limit reaching system sizes of the order of $L \approx 10^4$ with a relative error of approximately $\epsilon \approx 1\%$, where ϵ is the relative error of the average localization length after N TMM iterations. To compute the localization length at the Fermi level, we implemented TMM at the value of k_x at which the gap closes (calculated using the golden ratio search algorithm discussed in Appendix B). We have noticed that the valence band presents two local maxima, one around the Γ -point and the other around the M -point, however, the gap only closes around one of them. The TMM results in Fig. 1(c) is a sum of the localization lengths for the two local maxima, a quantity that diverges when either of the localization lengths does. For any other value of k_x , TMM will always give a finite but small ξ since the spectra of \mathcal{H}_{k_x} is gapped. With this approach, we compute the localization length ξ at $E = 0$ for a set of points (B, W) , thus obtaining in Fig. 1(c) the contour of the original topological phase diagram shown in Fig. 1(a). For high enough quasi-periodic potential strength, when $B \lesssim -3$ or $B \gtrsim 2$, this approach fails since the gap closes and does not reopen. The method of golden ratio search also fails in gapless regions since the gap closes at a continuous region of k_x .

To better understand the localization properties, we

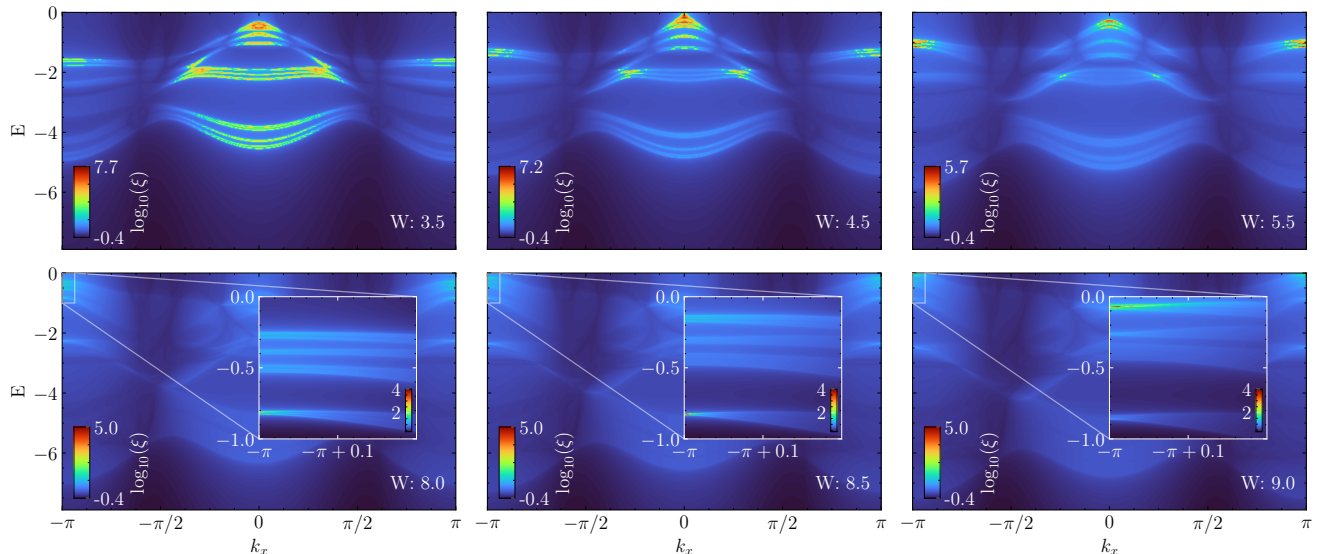


FIG. 2. Localization length as a function of energy E and momentum k_x at $B = -3$ for the entire range of the valence band. The grid discretization is 300×300 . The insets follow the same procedure for a smaller region ($E \in [-1, 0]$ and $k_x \in [-\pi, -\pi + 0.2]$) with a grid discretization of 600×600 .

have performed an energy-resolved study considering energies away from the Fermi level. Since localized bulk states do not contribute to the system's topological properties, analyzing the energy position of the extended bulk states with increasing quasi-periodic potential should give us some intuition on how they affect the topological phases. For regular Anderson disorder in 1D and 2D, any amount of disorder fully localizes the spectrum for systems belonging to the orthogonal symmetry class A [90]. As previously discussed, the same does not occur in incommensurate structures for which finite fractions of extended states can exist. To study the localization properties of the bulk states as a function of the energy E we computed the k_x and E resolved localization length, $\xi(k_x, E)$, for different values of the quasi-periodic potential.

In Fig. 2 the k_x -dependent results for the localization length can be seen for $B = -3$. For the first topological phase transition from $C = 2$ to $C = 1$ (upper panel) there is a set of extended states around $k_x = 0$, where the gap closes. We can clearly see that the higher the quasi-periodic potential W , the higher the fraction of localized states. On the lower panel of Fig. 2, we see that right before the second transition from $C = 1$ to $C = 0$, most of the bulk states are localized except for a few extended states, which we can observe if we use a fine enough grid discretization, as seen in the inset. In Appendix C we show, using inverse participation ratio calculations, that these few extended states are really extended and not critical. After the transition, at $W > 9$ all the states are Anderson localized, and the system is in a trivial Anderson insulating phase.

Figure 2 shows the localization length $\xi(k_x, E)$ for $B = -2$. For small W we can see that the QBCP is robust, as expected from previous results. Around $W = 3.5$, we see that the QBCP splits into two Dirac points around the Γ point, while under increasing quasi-periodic potential strength, bulk states become increasingly more localized. In the lower panel of Fig. 2, we show the localization length results for a topological phase transition from $C = 1$ into a trivial phase. The gap closes at the transition, after which all the states fully localize. Overall, the same behavior follows for other values of B . On the other side of the diagram, $B > -1$, the behavior is similar, with a shift of $\Delta k_x = \pi$.

IV. DISCUSSION

In this work, we unveiled the complete phase diagram of a 2D system with a QBCP under an applied 1D quasi-periodic potential. In the following, we discuss our main results, comparing them with previous findings for the disordered QBCP system.

In the homogeneous limit, topological phase transitions occur when the gap closes at a QBCP. When a small quasi-periodic potential is applied, the y -direction is no longer translational invariant. Nonetheless, topological phase transitions are associated with the gap closing in a quadratic dispersion along k_x , as seen in Figs. 2 and 3. Moreover, these transitions occur through a gap-closing and reopening mechanism, as in the clean case, which strongly indicates that the QBCP is stable under the addition of quasi-periodic modulations. This be-

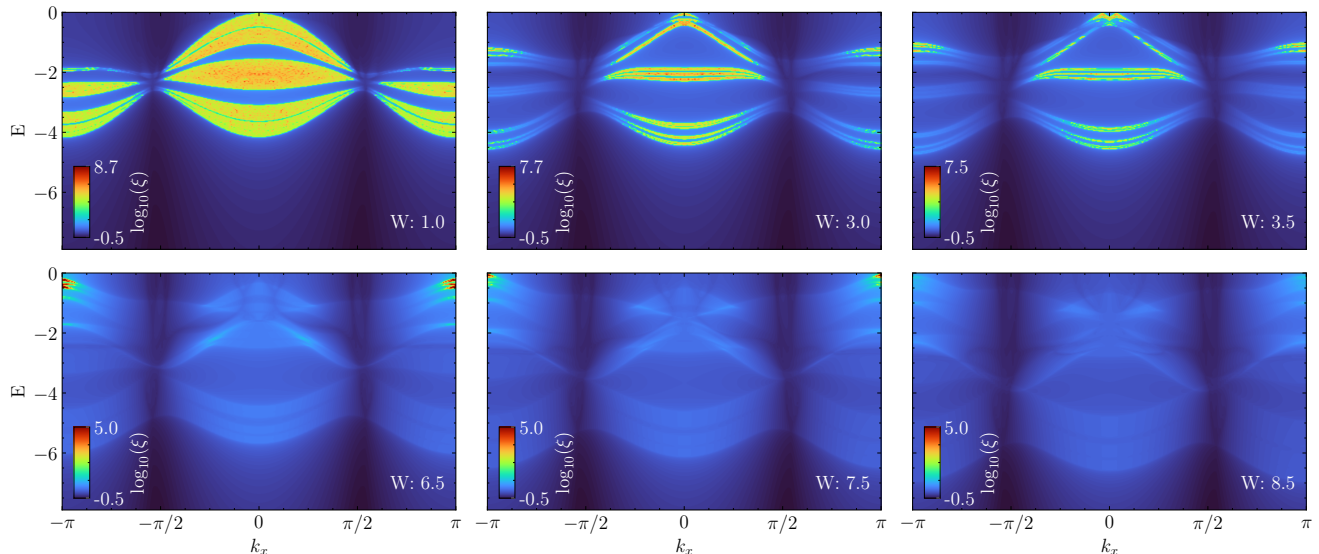


FIG. 3. Localization length as a function of energy E and momentum k_x at $B = -3$ for the entire range of the valence band. The grid discretization is 300×300 .

havior contrasts with the disordered case, for which the QBCP is unstable to the appearance of gapless phases with Chern numbers $C = \pm 1$, not present in the clean limit [79]. Interestingly, in the quasi-periodic case, topological transitions into $C = \pm 1$ phases were also observed for larger quasi-periodic potentials. However, unlike the disordered case, these transitions occur via a gap-closing and reopening mechanism. For the topological transitions from $C = \pm 2$ to $C = \pm 1$, one of the QBCP is split into two gapped Dirac cones (see, for instance, the upper right panel in Fig. 3), and the gap closes only at one of them (otherwise the Chern variation would be larger than one) [91]. In Fig. 2 (upper, middle panel), the Dirac cone at a gap closing point. Once again, unlike the disordered case, at very high potential strengths ($W \gtrsim 9$), the $C = \pm 1$ phases become gapless (with localized states at the Fermi level).

We also found the localization properties very distinct from the disordered case at small quasi-periodic potential. In the presence of disorder, most eigenstates are localized except for extended states that live on narrow energy windows. As for the quasi-periodic case, large clusters of bulk states remain extended. Furthermore, at high potential strengths, an analogous of the “levitation and annihilation” mechanism can be observed close to the transitions from the $C = \pm 1$ phases into the trivial phase. In fact, in this large potential limit, the $C = \pm 1$ phases can become gapless, with extended states only existing at very narrow energy windows [92]. As in the disordered case, all states localize after the topological transition into the trivial phase. Therefore, the topological and localization properties show a mixture of features commonly observed in the homogeneous and disor-

dered cases, as was previously observed for quasi-periodic Chern insulators in Ref. [78]. The small potential results are also in agreement with Ref. [82], where a different QBCP system was found to an (in this case fully two-dimensional) quasi-periodic potential. Our findings can be verified in ultracold atoms and trapped ions experiments, where quasi-periodic potentials are routinely implemented [50–59]. By keeping translational invariance along one direction, our study of a 1D quasi-periodic potential was a suitable starting point to address the interplay between quasi-periodicity and quadratic band crossings. However, an equally interesting question lies on the fate of the QBCP under the application of a fully two-dimensional quasi-periodic potential, that we leave for future exploration.

The authors acknowledge partial support from Fundação para a Ciência e Tecnologia (FCT-Portugal) through Grant No. UIDB/04650/2020. MG acknowledges partial support from Fundação para a Ciência e Tecnologia (FCT-Portugal) through Grant No. UID/CTM/04540/2019. MG acknowledges further support from FCT-Portugal through the Grant SFRH/BD/145152/2019.

Appendix A: Real Space and k_x -dependent Hamiltonian

In this section we present the k_x -dependent Hamiltonian. We start from the Hamiltonian written in the real space basis and take plane wave solutions along the invariant direction x , which enables us to reach far closer to thermodynamic limit. This transformation comes with

some caveats, since to have the full picture of the 2D system one needs to consider the entirety FBZ along the invariant direction, and so when computing gaps, for example, one needs to know exactly at which k_x does the

gap close. The real space Hamiltonian is: II.

$$\mathcal{H} = \mathcal{H}_0 + \mathcal{H}_B + \mathcal{H}_{1D}$$

Where each term is defined by:

$$\begin{aligned} \mathcal{H}_0 = \sum_{\mathbf{R}} \{ & t_z (|\mathbf{R} \pm a\hat{e}_x, A\rangle \langle \mathbf{R}, A| - |\mathbf{R} \pm a\hat{e}_y, A\rangle \langle \mathbf{R}, A|) - \\ & - t_z (|\mathbf{R} \pm a\hat{e}_x, B\rangle \langle \mathbf{R}, B| + |\mathbf{R} \pm a\hat{e}_y, B\rangle \langle \mathbf{R}, B|) + \\ & + \frac{t_x}{2} (|\mathbf{R} \pm a\hat{e}_x \pm a\hat{e}_y, A\rangle \langle \mathbf{R}, B| - |\mathbf{R} \pm a\hat{e}_x \mp a\hat{e}_y, A\rangle \langle \mathbf{R}, B|) + \\ & + \frac{t_x}{2} (|\mathbf{R} \pm a\hat{e}_x \pm a\hat{e}_y, B\rangle \langle \mathbf{R}, A| - |\mathbf{R} \pm a\hat{e}_x \mp a\hat{e}_y, B\rangle \langle \mathbf{R}, A|) \} \end{aligned}$$

$$\begin{aligned} \mathcal{H}_B = \sum_{\mathbf{R}} \{ & i (|\mathbf{R}, B\rangle \langle \mathbf{R}, A| - |\mathbf{R}, A\rangle \langle \mathbf{R}, B|) \\ & - i \frac{B+1}{4} (|\mathbf{R} \pm a\hat{e}_x, A\rangle \langle \mathbf{R}, B| + |\mathbf{R} \pm a\hat{e}_y, A\rangle \langle \mathbf{R}, B|) \\ & + i \frac{B+1}{4} (|\mathbf{R}, B\rangle \langle \mathbf{R} \pm a\hat{e}_x, A| + |\mathbf{R}, B\rangle \langle \mathbf{R} \pm a\hat{e}_y, A|) \} \end{aligned}$$

$$\mathcal{H}_{1D} = \frac{W}{2} \sum_{\mathbf{R}} \cos(2\pi\beta na) \{ |\mathbf{R}, A\rangle \langle \mathbf{R}, A| + |\mathbf{R}, B\rangle \langle \mathbf{R}, B| \}$$

We can now make a change of basis along the invariant

direction, using $|m, \alpha\rangle = \frac{1}{\sqrt{L_x}} \sum_{k_x} e^{-ik_x ma} |k_x, \alpha\rangle$ and obtain the 1D hamiltonian $\mathcal{H} = \sum_{k_x} \mathcal{H}(k_x) |k_x\rangle \langle k_x|$

$$\mathcal{H}(k_x) = \mathcal{H}_0(k_x) + \mathcal{H}_B(k_x) + \mathcal{H}_{1D}(k_x)$$

where:

$$\begin{aligned} \mathcal{H}_0(k_x) = \sum_n \{ & t_z (2 \cos(k_x a) |n, A\rangle \langle n, A| - |n \pm 1, A\rangle \langle n, A|) + \\ & + t_z (-2 \cos(k_x a) |n, B\rangle \langle n, B| + |n \pm 1, B\rangle \langle n, B|) + \\ & + it_x \sin(k_x a) (|n+1, A\rangle \langle n, B| - |n-1, A\rangle \langle n, B|) + \\ & + it_x \sin(k_x a) (|n+1, B\rangle \langle n, A| - |n-1, B\rangle \langle n, A|) \} \end{aligned}$$

$$\begin{aligned} \mathcal{H}_B(k_x) = \sum_n \{ & i (|n, B\rangle \langle n, A| - |n, A\rangle \langle n, B|) - \\ & - i \frac{B+1}{4} (2 \cos(k_x a) |n, A\rangle \langle n, B| + |n \pm 1, A\rangle \langle n, B|) + \\ & + i \frac{B+1}{4} (2 \cos(k_x a) |n, B\rangle \langle n, A| + |n, B\rangle \langle n \pm 1, A|) \} \end{aligned}$$

$$\mathcal{H}_{1D}(k_x) = \frac{W}{2} \sum_n \cos(2\pi a\beta n) \{|n, A\rangle\langle n, A| + |n, B\rangle\langle n, B|\}$$

Appendix B: Golden ratio Search Method

Here we present the Golden Ratio Search method, implemented to compute the local maximum/minimum of a function of one variable $f(x)$. The simplest implementation of the method only computes local or global minima. However taking $f(x) \rightarrow -f(x)$ one can compute the maxima of the function $f(x)$.

1. Choose two initial outside points x_1 and x_4 , compute two interior points $x_2 = x_4 - (x_4 - x_1)/z$ and $x_3 = x_1 + (x_4 - x_1)/z$ (Golden Ratio Rule), then evaluate $f(x)$ at each of the points and set a target accuracy ϵ for the position of the minimum.
2. If $f(x_2) < f(x_3)$ then the minimum lies between x_1 and x_3 . Each point is shifted such that x_3 becomes the new x_4 , x_2 becomes the new x_3 and the new x_2 is computed using the Golden Ratio Rule. Evaluate $f(x)$ at the new point.
3. Otherwise, the minimum lies between x_2 and x_4 . Each point is shifted such that x_2 becomes the new x_1 , x_3 becomes the new x_2 and the new x_3 is computed using the Golden Ratio Rule. Evaluate $f(x)$ at the new point.
4. If $x_4 - x_1 > \epsilon$ repeat from step 2. Otherwise the final estimate of the position of the minimum is $\frac{1}{2}(x_2 + x_3)$.

The value of z on the Golden Ratio Rule can be any value from $]0, 1[$, however the value of z that lets the method converge in the least amount of iterations is $z = \frac{1+\sqrt{5}}{2}$, the Golden Ratio. One can now implement this algorithm to maximize $E_-(k_x)$.

Appendix C: IPR and Fractal Dimension

Here we corroborate the results obtained via TMM at the insets of Fig. 2. We consider the IPR scaling with system size L and compute the fractal dimension ν for the three eigenstates with bigger localization length.

We confirm that overall these states are always fully extended, yielding $\nu \approx 1$. For the states that have smaller fractal dimension we still conclude that they are extended since ν approaches 1 for the larger system sizes.

-
- [1] M. Z. Hasan and C. L. Kane, *Rev. Mod. Phys.* **82**, 3045 (2010).
 - [2] X.-L. Qi and S.-C. Zhang, *Rev. Mod. Phys.* **83**, 1057 (2011).
 - [3] B. A. B. with Taylor L. Hughes, *Topological Insulators and Topological Superconductors* (Princeton University Press, 2013).
 - [4] C.-K. Chiu, J. C. Y. Teo, A. P. Schnyder, and S. Ryu, *Rev. Mod. Phys.* **88**, 035005 (2016).
 - [5] K. V. Klitzing, G. Dorda, and M. Pepper, *Physical Review Letters* **45**, 494 (1980).
 - [6] D. J. Thouless, M. Kohmoto, M. P. Nightingale, M. D. Nijs, and M. den Nijs, *Phys. Rev. Lett.* **49**, 405 (1982).
 - [7] Q. Niu, D. J. Thouless, and Y.-S. Wu, *Phys. Rev. B* **31**, 3372 (1985).
 - [8] F. D. M. Haldane, *Phys. Rev. Lett.* **61**, 2015 (1988).
 - [9] C.-Z. Chang, J. Zhang, X. Feng, J. Shen, Z. Zhang, M. Guo, K. Li, Y. Ou, P. Wei, L.-L. Wang, Z.-Q. Ji, Y. Feng, S. Ji, X. Chen, J. Jia, X. Dai, Z. Fang, S.-C. Zhang, K. He, Y. Wang, L. Lu, X.-C. Ma, and Q.-K. Xue, *Science* **340**, 167 (2013).
 - [10] G. Jotzu, M. Messer, R. Desbuquois, M. Lebrat, T. Uehlinger, D. Greif, and T. Esslinger, *Nature* **515**, 237 (2014).
 - [11] J. G. Checkelsky, R. Yoshimi, A. Tsukazaki, K. S. Takahashi, Y. Kozuka, J. Falson, M. Kawasaki, and Y. Tokura, *Nature Physics* **10**, 731 (2014).
 - [12] C. Z. Chang, W. Zhao, D. Y. Kim, H. Zhang, B. A. Assaf, D. Heiman, S. C. Zhang, C. Liu, M. H. Chan, and J. S. Moodera, *Nature Materials* **14**, 473 (2015).
 - [13] A. H. Castro Neto, F. Guinea, N. M. Peres, K. S. Novoselov, and A. K. Geim, *Reviews of Modern Physics* **81**, 109 (2009).
 - [14] K. Sun, H. Yao, E. Fradkin, and S. A. Kivelson, *Phys. Rev. Lett.* **103**, 46811 (2009), arXiv:0905.0907.
 - [15] S. Uebelacker and C. Honerkamp, *Phys. Rev. B* **84**, 205122 (2011).
 - [16] J. M. Murray and O. Vafek, *Phys. Rev. B* **89**, 201110 (2014).
 - [17] S. Ray, M. Vojta, and L. Janssen, *Phys. Rev. B* **98**, 245128 (2018), arXiv:1810.07695.
 - [18] T. S. Zeng, W. Zhu, and D. Sheng, *npj Quantum Mater.* **3**, 49 (2018), arXiv:1805.01101.
 - [19] D. Xiao, M. C. Chang, and Q. Niu, *Reviews of Modern Physics* **82**, 1959 (2010).
 - [20] B. Kramer and A. MacKinnon, *Rep. Prog. Phys.* **56**, 1469 (1993).
 - [21] M. Onoda and N. Nagaosa, *Phys. Rev. Lett.* **90**, 206601 (2003).
 - [22] M. Onoda, Y. Avishai, and N. Nagaosa, *Phys. Rev. Lett.* **98**, 76802 (2007).
 - [23] E. Prodan, T. L. Hughes, and B. A. Bernevig, *Phys. Rev. Lett.* **105**, 115501 (2010).

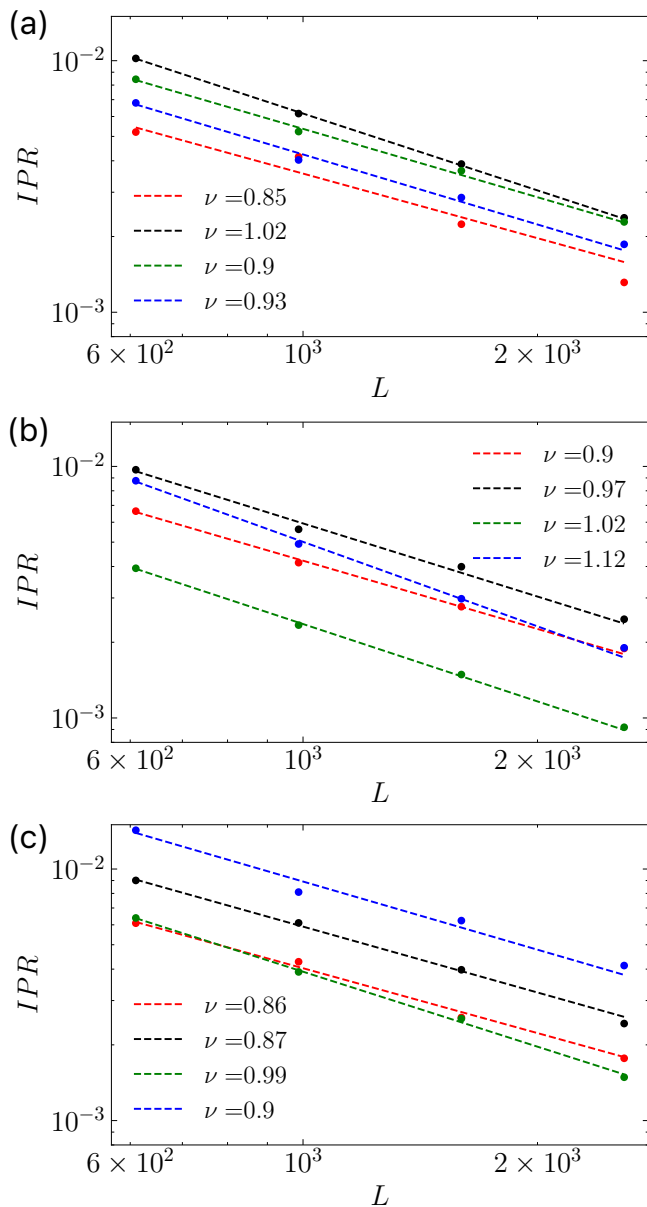


FIG. 4. IPR values of the three states with the biggest localization length obtained with TMM for $B = -3$. The fractal dimension was estimated for each pair of (E, k_x) . (a) $W = 8.0$; (b) $W = 8.5$; (c) $W = 9.0$

- [24] E. Prodan, *Journal of Physics A: Mathematical and Theoretical* **44**, 113001 (2011).
- [25] E. V. Castro, M. P. López-Sancho, and M. A. Vozmediano, *Physical Review B - Condensed Matter and Materials Physics* **92** (2015), 10.1103/PhysRevB.92.085410.
- [26] J. Li, R.-L. Chu, J. K. Jain, and S.-Q. Shen, *Phys. Rev. Lett.* **102**, 136806 (2009).
- [27] C. W. Groth, M. Wimmer, A. R. Akhmerov, J. Tworzydło, and C. W. Beenakker, *Physical Review Letters* **103**, 196805 (2009).
- [28] J. Song, H. Liu, H. Jiang, Q. F. Sun, and X. C. Xie, *Physical Review B - Condensed Matter and Materials Physics* **85** (2012), 10.1103/PhysRevB.85.195125.
- [29] J. H. García, L. Covaci, and T. G. Rappoport, *Physical Review Letters* **114**, 1 (2015).
- [30] C. P. Orth, T. Sekera, C. Bruder, and T. L. Schmidt, *Scientific Reports* **6** (2016), 10.1038/srep24007.
- [31] M. Gonçalves, P. Ribeiro, and E. V. Castro, “The haldane model under quenched disorder,” (2018).
- [32] M. Johansson and R. Riklund, *Phys. Rev. B* **43**, 13468 (1991).
- [33] J. Biddle and S. Das Sarma, *Phys. Rev. Lett.* **104**, 70601 (2010).
- [34] J. D. Bodyfelt, D. Leykam, C. Danieli, X. Yu, and S. Flach, *Phys. Rev. Lett.* **113**, 236403 (2014).
- [35] F. Liu, S. Ghosh, and Y. D. Chong, *Phys. Rev. B - Condens. Matter Mater. Phys.* **91**, 014108 (2015).
- [36] C. Danieli, J. D. Bodyfelt, and S. Flach, *Phys. Rev. B* **91**, 235134 (2015).
- [37] S. Ganeshan, J. H. Pixley, and S. Das Sarma, *Phys. Rev. Lett.* **114**, 146601 (2015).
- [38] T. Liu, X. Xia, S. Longhi, and L. Sanchez-Palencia, *SciPost Phys.* **12**, 27 (2022).
- [39] M. Gonçalves, B. Amorim, E. V. Castro, and P. Ribeiro, (2022), 10.48550/arxiv.2206.13549, arXiv:2206.13549.
- [40] M. Gonçalves, B. Amorim, E. V. Castro, and P. Ribeiro, “Critical phase in a class of 1d quasiperiodic models with exact phase diagram and generalized dualities,” (2022).
- [41] C. Huang, F. Ye, X. Chen, Y. V. Kartashov, V. V. Konotop, and L. Torner, *Scientific Reports* **6**, 32546 (2016).
- [42] J. H. Pixley, J. H. Wilson, D. A. Huse, and S. Gopalakrishnan, *Phys. Rev. Lett.* **120**, 207604 (2018).
- [43] M. J. Park, H. S. Kim, and S. Lee, *Phys. Rev. B* **99**, 245401 (2019), arXiv:1812.09170.
- [44] P. Bordia, H. Lüschen, S. Scherg, S. Gopalakrishnan, M. Knap, U. Schneider, and I. Bloch, *Phys. Rev. X* **7**, 041047 (2017).
- [45] B. Huang and W. V. Liu, *Phys. Rev. B* **100**, 144202 (2019).
- [46] Y. Fu, E. J. König, J. H. Wilson, Y.-Z. Chou, and J. H. Pixley, *npj Quantum Materials* **5**, 71 (2020).
- [47] Y.-Z. Chou, Y. Fu, J. H. Wilson, E. J. König, and J. H. Pixley, *Phys. Rev. B* **101**, 235121 (2020).
- [48] P. Wang, Y. Zheng, X. Chen, C. Huang, Y. V. Kartashov, L. Torner, V. V. Konotop, and F. Ye, *Nature* **577**, 42 (2020).
- [49] M. Gonçalves, H. Z. Olyaei, B. Amorim, R. Mondaini, P. Ribeiro, and E. V. Castro, *2D Materials* **9**, 011001 (2021).
- [50] D. J. Boers, B. Goedeke, D. Hinrichs, and M. Holthaus, *Phys. Rev. A* **75**, 63404 (2007).
- [51] G. Roati, C. D’Errico, L. Fallani, M. Fattori, C. Fort, M. Zaccanti, G. Modugno, M. Modugno, and M. Inguscio, *Nature* **453**, 895 (2008), arXiv:0804.2609.
- [52] M. Modugno, *New Journal of Physics* **11**, 33023 (2009).
- [53] M. Schreiber, S. S. Hodgman, P. Bordia, H. P. Lüschen, M. H. Fischer, R. Vosk, E. Altman, U. Schneider, and I. Bloch, *Science* **349**, 842 (2015), arXiv:1501.05661.
- [54] H. P. Lüschen, S. Scherg, T. Kohlert, M. Schreiber, P. Bordia, X. Li, S. Das Sarma, and I. Bloch, *Phys. Rev. Lett.* **120**, 160404 (2018).
- [55] H. Yao, H. Khoudli, L. Bresque, and L. Sanchez-Palencia, *Phys. Rev. Lett.* **123**, 070405 (2019).
- [56] H. Yao, T. Giamarchi, and L. Sanchez-Palencia, *Phys. Rev. Lett.* **125**, 060401 (2020).
- [57] R. Gautier, H. Yao, and L. Sanchez-Palencia, *Phys. Rev. Lett.* **126**, 110401 (2021).

- [58] F. A. An, K. Padavić, E. J. Meier, S. Hegde, S. Ganeshan, J. H. Pixley, S. Vishveshwara, and B. Gadway, *Phys. Rev. Lett.* **126**, 040603 (2021).
- [59] T. Kohler, S. Scherg, X. Li, H. P. Lüschen, S. Das Sarma, I. Bloch, and M. Aidelsburger, *Phys. Rev. Lett.* **122**, 170403 (2019).
- [60] Y. Lahini, R. Pugatch, F. Pozzi, M. Sorel, R. Morandotti, N. Davidson, and Y. Silberberg, *Phys. Rev. Lett.* **103**, 013901 (2009).
- [61] Y. E. Kraus and O. Zilberberg, *Phys. Rev. Lett.* **109**, 116404 (2012).
- [62] M. Verbin, O. Zilberberg, Y. E. Kraus, Y. Lahini, and Y. Silberberg, *Phys. Rev. Lett.* **110**, 076403 (2013).
- [63] M. Verbin, O. Zilberberg, Y. Lahini, Y. E. Kraus, and Y. Silberberg, *Phys. Rev. B* **91**, 64201 (2015).
- [64] A. D. Sinelnik, I. I. Shishkin, X. Yu, K. B. Samusev, P. A. Belov, M. F. Limonov, P. Ginzburg, and M. V. Rybin, *Advanced Optical Materials* **8**, 2001170 (2020), <https://onlinelibrary.wiley.com/doi/pdf/10.1002/adom.202001170>
- [65] P. Wang, Q. Fu, R. Peng, Y. V. Kartashov, L. Torner, V. V. Konotop, and F. Ye, *Nature Communications* **13**, 6738 (2022).
- [66] D. J. Apigo, W. Cheng, K. F. Dobiszewski, E. Prodan, and C. Prodan, *Phys. Rev. Lett.* **122**, 095501 (2019).
- [67] X. Ni, K. Chen, M. Weiner, D. J. Apigo, C. Prodan, A. Alù, E. Prodan, and A. B. Khanikaev, *Communications Physics* **2**, 55 (2019).
- [68] W. Cheng, E. Prodan, and C. Prodan, *Phys. Rev. Lett.* **125**, 224301 (2020).
- [69] Y. Xia, A. Erturk, and M. Ruzzene, *Phys. Rev. Applied* **13**, 014023 (2020).
- [70] Z.-G. Chen, W. Zhu, Y. Tan, L. Wang, and G. Ma, *Phys. Rev. X* **11**, 011016 (2021).
- [71] M. Gei, Z. Chen, F. Bosi, and L. Morini, *Applied Physics Letters* **116**, 241903 (2020), <https://doi.org/10.1063/5.0013528>.
- [72] L. Balents, C. R. Dean, D. K. Efetov, and A. F. Young, *Nat. Phys.* **16**, 725 (2020).
- [73] E. Y. Andrei and A. H. MacDonald, *Nature Materials* **19**, 1265 (2020).
- [74] A. Uri, S. C. de la Barrera, M. T. Randeria, D. Rodan-Legrain, T. Devakul, P. J. D. Crowley, N. Paul, K. Watanabe, T. Taniguchi, R. Lifshitz, L. Fu, R. C. Ashoori, and P. Jarillo-Herrero, “Superconductivity and strong interactions in a tunable moiré quasiperiodic crystal,” (2023), [arXiv:2302.00686 \[cond-mat.mes-hall\]](https://arxiv.org/abs/2302.00686).
- [75] Y. Fu, J. H. Wilson, and J. H. Pixley, *Physical Review B* **104** (2021), 10.1103/physrevb.104.1041106.
- [76] S. Cheng, R. Asgari, and G. Xianlong, *Physical Review B* **108**, 024204 (2023), [arXiv:2212.04082](https://arxiv.org/abs/2212.04082).
- [77] M. F. Madeira and P. D. Sacramento, *Phys. Rev. B* **106**, 224505 (2022).
- [78] T. S. Gonçalves, M. Gonçalves, P. Ribeiro, and B. Amorim, “Topological phase transitions for any taste in 2d quasiperiodic systems,” (2022), [arXiv:2212.08024 \[cond-mat.dis-nn\]](https://arxiv.org/abs/2212.08024).
- [79] N. Sobrosa, M. Gonçalves, and E. V. Castro, (2021).
- [80] J. Wang, C. Ortix, J. van den Brink, and D. V. Efremov, *Phys. Rev. B* **96**, 201104 (2017), [arXiv:1710.09632](https://arxiv.org/abs/1710.09632).
- [81] Y.-M. Dong, Y.-H. Zhai, D.-X. Zheng, and J. Wang, *Phys. Rev. B* **102**, 134204 (2020).
- [82] J. Lee and J. H. Pixley, *SciPost Phys.* **13**, 033 (2022).
- [83] M. Gonçalves, H. Z. Olyaei, B. Amorim, R. Mondaini, P. Ribeiro, and E. V. Castro, *2D Materials* **9**, 011001 (2021).
- [84] T. Fukui, Y. Hatsugai, and H. Suzuki, *Journal of the Physical Society of Japan* **74**, 1674 (2005), <https://doi.org/10.1143/JPSJ.74.1674>.
- [85] Y.-F. Zhang, Y.-Y. Yang, Y. Ju, L. Sheng, R. Shen, D.-N. Sheng, and D.-Y. Xing, *Chinese Physics B* **22**, 117312 (2013).
- [86] A. Weiße, G. Wellein, A. Alvermann, and H. Fehske, *Rev. Mod. Phys.* **78**, 275 (2006).
- [87] A. Mackinnon and B. Kramer, *Phys. Rev. Lett.* **47**, 1546 (1981).
- [88] A. MacKinnon and B. Kramer, *Zeitschrift für Physik B Condensed Matter* **53**, 1 (1983).
- [89] At general k_x the spectrum of \mathcal{H}_{k_x} is gapped, thus one might conclude that the system is gapped if the proper k_x is not chosen.
- [90] E. Abrahams, P. W. Anderson, D. C. Licciardello, and T. V. Ramakrishnan, *Phys. Rev. Lett.* **42**, 673 (1979).
- [91] While each QBCP gives contributions $\Delta C = \pm 1$ to the Chern number, each Dirac cone only contributes with $\Delta C = \pm 1/2$. When the gap closes and reopens at a given Dirac cone, the sign of its contribution changes, canceling with the unchanged contribution of the remaining cone. As a result, there is a net change of $\Delta C = \pm 1$ and we enter the $C = \pm 1$ phases.
- [92] Interestingly, these narrow extended states arise even slightly before the gap closes.